IMPROVING FLUORESCENCE LIFETIME IMAGING MICROSCOPY DECONVOLUTION USING CONSTRAINED LAGUERRE BASIS FUNCTIONS

A Thesis

by

MOHAMMED IBRAHIM KHATKHATAY

Submitted to the Office of Graduate and Professional Studies of
Texas A&M University
in partial fulfillment of the requirements for the degree of

MASTER OF SCIENCE

Chair of Committee,	Javier A. Jo
Co-Chair of Committee,	Brian E. Applegate
Committee Member,	Jim Ji
Head of Department,	Gerard E. Coté

May 2014

Major Subject: Biomedical Engineering

ABSTRACT

Fluorescence lifetime imaging microscopy (FLIM) is a noninvasive invasive optical imaging modality which is finding new applications in medical imaging. In FLIM, the fluorescence time decay is measured at a pixel. The fluorescence impulse response function (IRF) is then estimated using a deconvolution of the instrument response and the measured fluorescence time decay. Two of the challenges facing FLIM are speed of the deconvolution and the accuracy of the IRFs.

The linear expansion of the fluorescence decays based on the orthonormal Laguerre basis functions (LBFs) is among the fastest methods for estimating the IRFs. The automated implementation to optimize the Laguerre parameter improves the speed of the deconvolution using the LBFs but uses a global optimization. Therefore, the IRFs do not necessarily mimic exponential time decays, or monotonically decreasing functions. On the other hand, applying a constraint to the LBFs using the Active Set Nonnegative Least Squares (NNLS) method improves the IRF estimation. The estimation of the Laguerre parameter using the NNLS method, however, is about 10-15x slower. By combining these two deconvolution techniques, we found that the deconvolution time is similar to the automated global Laguerre parameter deconvolution while the IRF estimation always results in a monotonically decreasing function.

DEDICATION

I dedicate this thesis to my mother, Kishwar Joonas Khatkhatay, and my sister, Fauzia Khatkhatay, who have always advised and supported me no matter what challenge came my way and, when needed, pushed me to greater heights.

ACKNOWLEDGEMENTS

I would like to express my gratitude to my committee chair and co-chair, Drs. Jo and Applegate, and committee member, Dr. Ji, for their continued guidance, support, and flexibility throughout the course of this research.

I would also like to thank my lab members for their time and effort in helping me understand the material with which I struggled and my fellow graduate students for the interesting and engaging dialogues we had.

NOMENCLATURE

FLIM	Fluorescence Lifetime Imaging Microscopy
IRF	Impulse Response Function
FWHM	Full-Width Half-Max
BP	Bandpass Filter
B[a]P	Benza[a]pyrene
SCC	Squamous Cell Carcinoma
LBFs	Laguerre Basis Functions
n	Derivative Order
OLS	Ordinary Least-Squares Fitting
CLS-n	n-th Derivative Constrained Least-Squares Fitting
α_{OLS}	α Optimized Using the Linear Least-Squares Fitting Laguerre Method
α_{CLS-n}	α Optimized Using an Iterative Method for the n-th Derivative Constrained Least-Squares Fitting Laguerre Method
Modified OLS-n	Method Combining the Ordinary Least-Squares Fitting and n-th Derivative Constrained Least-Squares Fitting Laguerre Methods

TABLE OF CONTENTS

Page

LIST OF FIGURES

Page

LIST OF TABLES

Page

1. INTRODUCTION

Multispectral fluorescence lifetime imaging (multispectral FLIM) has gained recognition over the last decade as a noninvasive optical imaging modality but with only limited applications in clinical imaging [1-5]. Many of the limitations have been addressed and improved upon within the last decade [6-9], but some limitations still remain. One of these limitations is the improper deconvolution of the fluorescence decays within the data set. We aim to address this issue by constraining the deconvolution method for the analysis of Fluorescence Lifetime Imaging Microscopy (FLIM) data for better fitting and decays while minimizing the time required for processing.

In time-domain FLIM, the recorded decay at a given pixel of the FLIM image can be mathematically modeled as a convolution of the instrument response with the Impulse Response Function (IRF) of the sample at that pixel (Fig. 1). Therefore, in order to estimate the IRF, the instrument response must be deconvolved from the recorded fluorescence decay, which has intrinsic system noise added (Fig. 2).

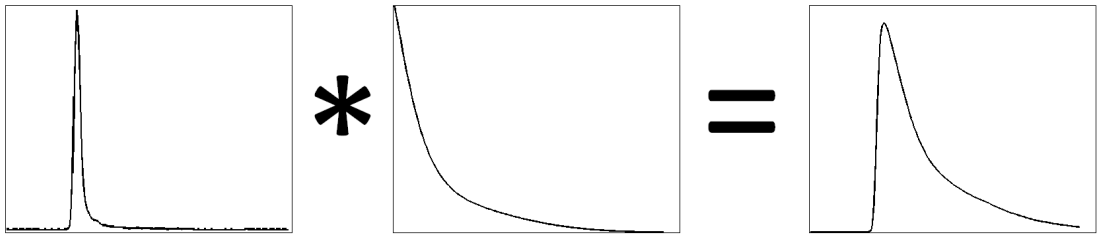

Figure 1: Example of Convolution. The instrument response is convolved with the IRF, resulting in the recorded fluorescence decay.

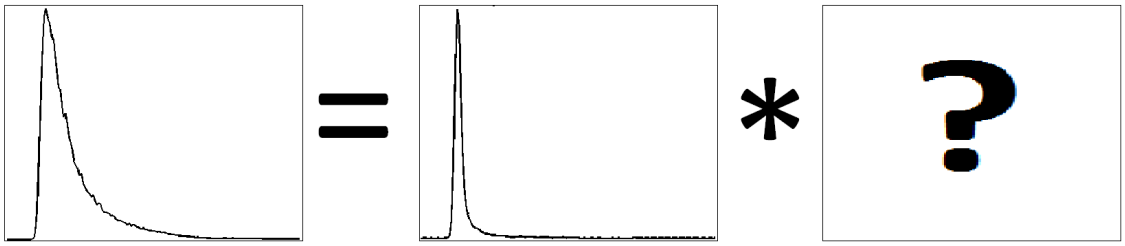

Figure 2: Example of Deconvolution. The Measured Fluorescence Decay is Noise-Corrupted, Resulting in a More Complex Deconvolution Process.

Among the most common deconvolution techniques are functions which model the IRF as a multi-exponential decay and estimates the lifetime and amplitude parameters iteratively [10] and functions which use a stretched exponential function [11]. Both techniques use a non-linear least squares optimization and require some *a priori* knowledge about the modeled exponentials. Similarly, most of the existing methods demand user intervention and are computationally expensive. These aspects result in time-consuming methods which cannot be used for real-time, or clinically relevant, applications.

Recently, FLIM deconvolution methods based on the linear expansion of the fluorescence decays on a set of orthonormal Laguerre functions have gained popularity [12-16]. An automated FLIM time-deconvolution method exists also based on the Laguerre method to optimize one of parameters, which results in a reduction of the required computation time [7]. The method estimates the expansion coefficients on all pixel decays using only one iteration and a linear least-square estimation, performing at least two orders of magnitude faster. The method uses an *a priori* number of orthonormal bases and optimizes the decay rate, referred to as the Laguerre parameter. However, the method is a global optimization and as such uses the entire data set. The global optimization achieves optimal fitting for the majority of the IRFs in the data set but with the possibility of local spatial area abnormalities. To overcome this limitation, we will apply a constraint to the FLIM time-deconvolution method based on the linear expansion of the fluorescence decays on an orthonormal Laguerre basis [17]. Our work will utilize the speed of the Laguerre deconvolution method while ensuring proper deconvolved decays.

2. METHODS

2.1 Multispectral FLIM

The FLIM data being used was acquired through a high-speed multispectral FLIM imaging system developed by Shrestha *et al.* [6], shown schematically in Fig. 3. The scanning FLIM system was implemented following a direct pulse-recording scheme, in which the pixel rate could be equal to the laser repetition rate. A frequency tripled Q-switched Nd:YAG laser was used as the excitation source (355 nm, 30 kHz maximum repetition rate, 1 ns pulse FWHM). The fluorescence emission was separated into three bands using a set of dichroic mirrors and filters (390 ± 20 nm for collagen, 452 ± 22.5 nm for elastin, and 550 ± 20 nm for lipids). Each band was launched into a fiber with different lengths (1 m, 10 m and 19 m, respectively), chosen to provide ~45 ns intervals between each emission band decay. The three consecutive decays were detected with a MCP-PMT (rise time: 150 ps) and sampled with a high bandwidth digitizer (1.5 GHz, 4 GS/s). The system lateral resolution was measured to be 100 μm. Each multispectral FLIM image (FOV: 2mm x 2mm at 60 pixels x 60 pixels) was acquired in ~7 s.

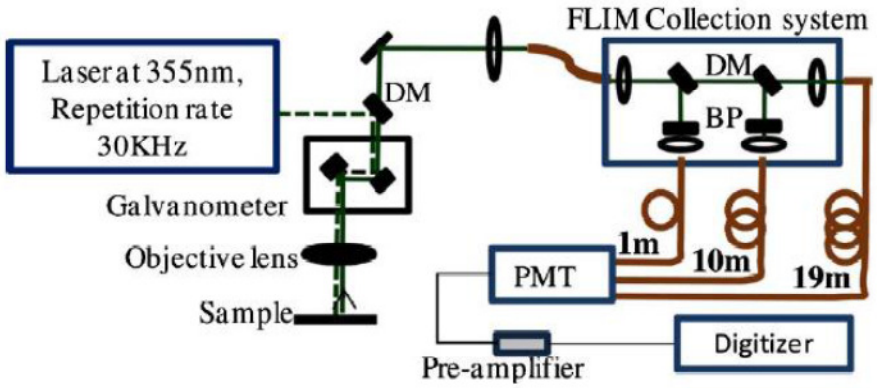

Figure 3: Schematic of the FLIM System. Dichroic mirrors guide the laser beam to the sample and the emission beam to the FLIM collection system: BP, bandpass filter; DM, dichroic mirror.

2.2 Tissue Specimens – Hamster Cheek Pouch Database

A Syrian hamster cheek pouch model was used for the oral cancer study. The protocol for the model was based on work done by Brandon et al. [18], who developed a protocol to produce squamous cell carcinomas in the hamster cheek pouch using Benzo[a]pyrene (B[a]P) as the carcinogen to allow for more predictable precancerous lesions. The imaging protocol was used to image 52 male Syrian hamsters (25 control, 27 treated) using the system described above [6]. Each animal was imaged at several points, resulting in about 250 FLIM datasets. After histology, the tissue imaged was classified as: 1) healthy, 2) hyperkeratosis (increase in the keratin layer), 3) hyperplasia (increase in the thickness of the epithelial layer due to an increased number of cells), 4) mild dysplasia, 5) moderate dysplasia, 6) severe dysplasia, and 7) Squamous Cell Carcinoma (SCC). As the current work only addresses signal processing, no comparisons were made to the tissue classification.

2.3 Deconvolution Using Laguerre Basis Functions (LBFs)

In the context of time-domain FLIM, the series of time-gated fluorescence intensity maps $H(r,n)$ are given by the convolution of Impulse Response Function (IRF) $h(r,n)$ with the instrument response $x(n)$:

$$H(r,n) = \sum_{m=0}^{K-1} h(r,m)x(n-m) \quad (1)$$

where r denotes the pixel location, n denotes the time gate ($n = 0,1,2 \ldots, N-1$), and K determines the extent of system memory [8]. The Laguerre deconvolution technique uses a set of Discrete Laguerre Functions (DLF) as the orthonormal basis to represent the IRF:

$$h(r,n) = \sum_{j=0}^{L-1} c_j(r) b_j^{\alpha}(n) \quad (2)$$

where, $c_j(r)$ are the unknown Laguerre Expansion Coefficients (LEC) at pixel r, $b_j^{\alpha}(n)$ denotes the j^{th} order DLF [8] defined as below:

$$b_j^{\alpha}(n) = \alpha^{\frac{n-j}{2}}(1-\alpha)^{\frac{1}{2}} \sum_{k=0}^{j} (-1)^k \binom{n}{k}\binom{j}{k} \alpha^{j-k}(1-\alpha)^k \quad (3)$$

and L, the Laguerre order, is the number of DLFs used to model the IRF. The Laguerre parameter ($0<\alpha<1$) determines the rate of exponential decline of the DLFs and defines the time scale for which the Laguerre expansion of the system IRF is most efficient in terms of convergence [9]. The DLF decays faster as α decreases (Fig. 4).

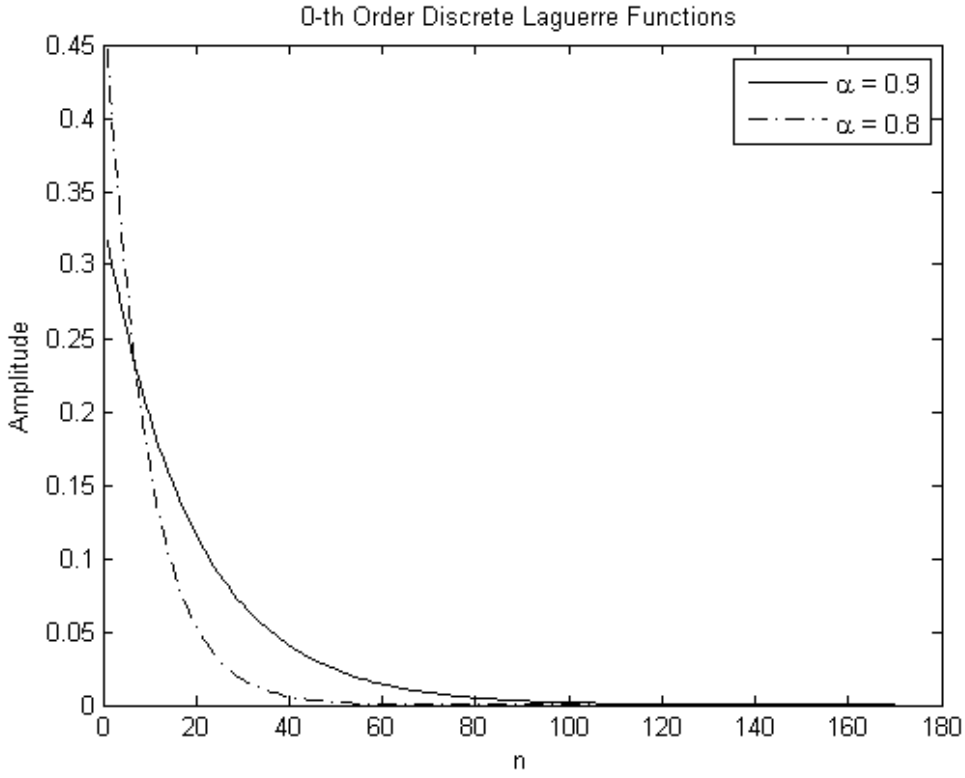

Figure 4: α-Dependence of Discrete Laguerre Functions (DLFs)

For a given pixel, the output $y(n)$ can thus be written as:

$$y(n) = H(r,n) = \sum_{j=0}^{L-1}\left[c_j(r)\underbrace{\left(\sum_{m=0}^{K-1} b_j^{\alpha}(m)x(n-m)\right)}_{v_j^{\alpha}(n)}\right] \quad (4)$$

Then, the system of linear equations defined in Equation 5 can be expressed in a matrix notation as follows:

$$\underbrace{\begin{bmatrix} y(0) \\ y(1) \\ \vdots \\ y(N-1) \end{bmatrix}}_{\bar{\boldsymbol{y}}} = \underbrace{\begin{bmatrix} v_0^{\alpha}(0) & \cdots & v_{L-1}^{\alpha}(0) \\ v_0^{\alpha}(1) & \cdots & v_{L-1}^{\alpha}(1) \\ \vdots & \ddots & \vdots \\ v_0^{\alpha}(N-1) & \cdots & v_{L-1}^{\alpha}(N-1) \end{bmatrix}}_{\boldsymbol{V}_{\alpha}} \underbrace{\begin{bmatrix} c_0 \\ c_1 \\ \vdots \\ \vdots \\ c_{L-1} \end{bmatrix}}_{\bar{\boldsymbol{c}}} + \epsilon \ (5)$$

We need to calculate the LEC vector, $\bar{\boldsymbol{c}}$, in order to obtain the IRF. The linear least-squares solution to $\bar{\boldsymbol{c}}$ is:

$$\bar{\boldsymbol{c}} = (\boldsymbol{V}_{\alpha}^{T}\boldsymbol{V}_{\alpha})^{-1}\boldsymbol{V}_{\alpha}\bar{\boldsymbol{y}} \ (6)$$

This solution, however, does not always result in an exponentially decreasing IRF. In order to modify the IRF, a constraint must be added.

2.4 Adding a Constraint to the LBFs

According to Liu et al [n], an IRF is referred to as an exponential decay (or monotonically decreasing function) if the function, h(t), for $0 \leq t \leq \infty$ follows the following requirements:

(i) $lim_{t\to\infty} h(t) = 0$

(ii) $h'(t) < 0$, and

(iii) $h''(t) > 0$,

where $h'(t)$ and $h''(t)$ are, respectively, the first and second derivatives of $h(t)$. These requirements translate into the dual problem

$$\min_{c\in R^L} \|\boldsymbol{y} - \boldsymbol{V}_\alpha \bar{\boldsymbol{c}}\|^2 \quad \text{subject to } (-1)^n \boldsymbol{D}^{(n)} \boldsymbol{B}_\alpha \bar{\boldsymbol{c}} \geq 0 \tag{7}$$

and

$$\min_{z\in R^{N-n}} \left\| \boldsymbol{C}\left(\boldsymbol{V}_\alpha^T \boldsymbol{y} + (-1)^n \boldsymbol{D}_\alpha^{(n)^T} \boldsymbol{z}\right)\right\|^2 \quad \text{subject to } \boldsymbol{z} \geq 0 \tag{8}$$

where $\boldsymbol{D}^{(n)}$ is the n-th order forward finite difference matrix [19], $\boldsymbol{C}$ is the Cholesky decomposition of the positive definite matrix $(\boldsymbol{V}_\alpha^T \boldsymbol{V}_\alpha)^{-1}$, and $\boldsymbol{D}_\alpha^{(n)} = \boldsymbol{D}^{(n)} \boldsymbol{B}_\alpha$. The constrained least-squares solution for $\bar{\boldsymbol{c}}$, $\bar{\boldsymbol{c}}_{CLS}^{(n)}$, of the IRF is

$$\bar{\boldsymbol{c}}_{CLS}^{(n)} = (\boldsymbol{V}_\alpha^T \boldsymbol{V}_\alpha)^{-1} \left(\boldsymbol{V}_\alpha^T \boldsymbol{y} + (-1)^n \boldsymbol{D}_\alpha^{(n)^T} \bar{\boldsymbol{z}}^{(n)}\right) \tag{9}$$

where $\bar{\mathbf{z}}^{(n)}$ is the solution to Equation 8, evaluated using an Active Set Non-Negative Least Squares (NNLS) [20]. As the definition for an exponential decay only requires the second derivative, the order, n, used for the NNLS method is also set to 2. However, because the third derivative has previously been published [17], both the second and third derivatives will be compared.

2.5 Methods and Parameters for Comparison

In order to compare the proposed constrained least-squares Laguerre method with existing Laguerre methods, we propose comparing each method by itself as well as combinations of the methods. The criteria for evaluation are the processing time required and whether the resulting IRF fits the definition of an exponential. The Laguerre parameter, α, is optimized using the method proposed by Pande et al. when using the linear least-squares Laguerre method [7]. However, when using the non-linear constrained least-squares Laguerre method, an iterative method is used to find the Laguerre parameter. The Laguerre parameter is determined to within a precision of 0.001. The Laguerre methods are also compared to a common biexponential method, as described below. Table 1 has the notations used to discuss the results.

Table 1: Notations

Notation	Meaning
OLS	Ordinary, or linear, least-squares
CLS-n	n-th derivative Constrained least-squares
α_{OLS}	α optimized using the Linear least-squares Laguerre method [23]
α_{CLS-n}	α optimized using an iterative method for the n-th derivative Constrained least-squares Laguerre method

All data sets are processed using MATLAB® 2013a on a destop running Windows 7 64-bit OS with an Intel® Core™2 Duo CPU @ 3.00GHz processor. All data set consist of three channels, each containing 3600 convolved curves and a representative instrument response curve. The instrument response curve is aligned with the majority of the convolved curves. All methods use five orthonormal LBFs (L=5). Studies have been conducted with a larger number of orthonormal LBFs. While a larger number of LBFs results in better fitting of the recorded fluorescence decay, the noise in the recorded fluorescence decay also affects the resulting deconvolved curve to a greater extent because of overfitting. The NNLS method is implemented using the lsqnonneg.m function. Table 2 has the methods which are tested along with the global optimization and deconvolution codes used for each method.

Table 2: Methods Tested

Method	Optimized Alpha Used	Deconvolving Code(s) Used
α_{OLS} with OLS	α_{OLS}	OLS Laguerre
α_{CLS-3} with CLS-3	α_{CLS-3}	CLS-3 Laguerre
α_{CLS-2} with CLS-2	α_{CLS-2}	CLS-2 Laguerre
α_{OLS} with CLS-3	α_{OLS}	CLS-3 Laguerre
α_{OLS} with CLS-2	α_{OLS}	CLS-2 Laguerre
Modified OLS-3	α_{OLS}	OLS Laguerre and CLS-3 Laguerre
Modified OLS-2	α_{OLS}	OLS Laguerre and CLS-2 Laguerre
Biexponential	--	Biexponential Estimation

The "Modified OLS-3" and "Modified OLS-2" methods use an *a priori* limit to decide whether the OLS Laguerre code results in an exponential decay. If the result is not an exponential decay, the curve is re-evaluated using the CLS Laguerre code. The *a priori* limit was found to be -3.2e+14 s^{-2} using the function

$$\min\left(\frac{\boldsymbol{D}^2 h(n)}{h_{max}(n) * (\Delta t)^2}\right) \quad (10)$$

where $\boldsymbol{D}^{(2)}$ is the second-order forward finite difference matrix [19], $h(n)$ is the deconvolved IRF for a given pixel, $h_{max}(n)$ is the maximum value of $h(n)$, and Δt is the sampling time. If (10) results in a value lower than the *a priori* limit, the curve is re-evaluated.

The "Biexponential" method estimates the IRF using the formula

$$h(n) = A_1 e^{-n\Delta t/\tau_1} + A_2 e^{-n\Delta t/\tau_2} \quad (11)$$

where A_1 and A_2 are the exponential decay coefficients and τ_1 and τ_2 are the lifetimes for the two exponential decays.

3. RESULTS AND DISCUSSION

3.1 Run Times Comparison

The time required to optimize the Laguerre parameter and deconvolve the curves in one data set is shown in Table 3, separated by channel (or fluorescence band). As expected, the "α_{CLS-3} with CLS-3" and "α_{CLS-2} with CLS-2" methods took over an order of magnitude longer than the "α_{OLS} with OLS" method to process. The reason for the increased time is due mainly to the iterative method of optimizing the Laguerre parameter and in part due to the non-negative least squares method used for the constraint. Also, the optimization process for these methods parsed the data set, using only 1 in 4 pixels. The "Biexponential" method also used a non-linear optimization and took around 5-6 times longer to process than the "α_{OLS} with OLS" method.

Table 3: Time Required to Process a Data Set (Separated by Channel). Row 1 represents 290nm, Row 2 Represents 452nm, and Row 3 Represents 520nm.

Method	α_{OLS} with OLS	α_{CLS-3} with CLS-3	α_{CLS-2} with CLS-2	α_{OLS} with CLS-3	α_{OLS} with CLS-2	Modified OLS-3	Modified OLS-2	Biexponential
Time Required to Optimize and Deconvolve Data Set (in sec, Mean ± SD)	8.1875 ± 0.7723	98.2766 ± 16.6738	89.7019 ± 11.3805	16.7718 ± 1.4389	15.8769 ± 1.4049	8.8770 ± 0.9565	8.8063 ± 0.8910	53.7339 ± 7.7396
	8.0355 ± 0.6665	113.3097 ± 15.6732	99.2588 ± 15.0895	16.7316 ± 1.4110	15.8144 ± 1.3631	8.7912 ± 1.5169	8.7535 ± 1.4210	47.2317 ± 7.0774
	8.4124 ± 0.3540	102.2207 ± 21.2903	97.0556 ± 19.0635	17.0753 ± 0.9068	16.2329 ± 0.6131	8.9874 ± 0.9033	8.9406 ± 0.7804	50.3208 ± 11.0607

The "α_{OLS} with CLS-3" and "α_{OLS} with CLS-2" methods took about twice as long as the "α_{OLS} with OLS" method to process, mainly due to the non-negative least squares method used for the constraint. The "Modified OLS-3" and "Modified OLS-2" methods took only slightly longer to process than the "α_{OLS} with OLS" method. These methods only corrected the fitting for those curves which did not follow the definition of an exponential decay curve; thus, the time required for processing using these methods was also reduced. Based on our data, the average percentage of curves in any channel which did not follow the definition of an exponential decay was about 3.95%, equivalent to 142 curves.

3.2 Error and Fitting Comparison

The fit of the modeled curve to the original data is determined by the error, ϵ, between the two curves as

$$\epsilon(r,n) = y(r,n) - \bar{y}(r,n) \quad (12)$$

where y is the convolved output and $\bar{y}$ is the convolved fit. The mean squared error, MSE, is determined by

$$MSE = \frac{1}{R * K} \sqrt{\sum_r \sum_n \epsilon(r,n)^2} \quad (13)$$

where R is the number of pixels and K determines the extent of system memory. Similarly, the normalized error, ϵ_{norm}, can be calculated by

$$\epsilon_{norm}(r,n) = \frac{y(r,n) - \bar{y}(r,n)}{y_{max}(r,n)} \quad (14)$$

where y_{max} is the maximum value of the convolved output of a curve, and the normalized mean squared error, MSE_{norm}, can be calculated by

$$MSE_{norm} = \frac{1}{R * K} \sqrt{\sum_{r} \sum_{n} \epsilon_{norm}(r,n)^2} \quad (15)$$

The normalized mean square error for a curve is shown in Table 4, separated by channel.

Table 4: Normalized Mean Square Error for a Convolved Curve (Separated by Channel). Row 1 represents 290nm, Row 2 Represents 452nm, and Row 3 Represents 520nm.

Method	α_{OLS} with OLS	α_{CLS-3} with CLS-3	α_{CLS-2} with CLS-2	α_{OLS} with CLS-3	α_{OLS} with CLS-2	Modified OLS-3	Modified OLS-2	Biexponential
Normalized Mean Squared Error (Mean ± SD)	0.0166 ± 0.0053	0.0178 ± 0.0053	0.0167 ± 0.0053	0.0180 ± 0.0056	0.0169 ± 0.0055	0.0170 ± 0.0057	0.0168 ± 0.0055	0.0177 ± 0.0050
	0.0154 ± 0.0055	0.0168 ± 0.0060	0.0156 ± 0.0057	0.0169 ± 0.0059	0.0157 ± 0.0056	0.0157 ± 0.0058	0.0155 ± 0.0056	0.1257 ± 0.0342
	0.0268 ± 0.0056	0.0278 ± 0.0061	0.0271 ± 0.0058	0.0277 ± 0.0060	0.0270 ± 0.0057	0.0270 ± 0.0057	0.0269 ± 0.0057	0.0276 ± 0.0058

All of the methods have similar errors and the "α_{OLS} with OLS" method has the lowest average normalized mean square error. The time required to process the methods, though, indicate that the "Modified OLS-3" and "Modified OLS-2" methods are preferable for comparison.

While the error fitting of the data set is important from a quantitative standpoint, the deconvolved curve itself is also important from a qualitative standpoint. Although the fluorescence curve fittings and their respective error fittings show a good fit for the models (Table 4 and Figs. 5-8), the deconvolved curves signify two improper deconvolution cases and one proper deconvolution case.

Figs. 5, 6, and 7 show the measured fluorescence and the fittings obtained from the four methods. The curve fittings in the first two cases for the "α_{OLS} with OLS" method (Figs. 5(a) and 7(a)) oscillate around the measured fluorescence as the curve decreases from the maximum value while the "Modified OLS-3" method fittings (Figs. 5(b) and 6(b)) and "Modified OLS-2" method fittings (Fig. 5(c) and 6(c)) do not oscillate around the measured fluorescence. The result of the "α_{OLS} with OLS" fitting for the third case (Fig. 7(a)) was determined to be above the *a priori* limit for the deconvolved curve and, therefore, was not reprocessed for "Modified OLS-3" and "Modified OLS-2" methods. The "Biexponential" method fittings (Figs. 5(d), 6(d), and 7(b)) are shown for comparison. Fig. 9 shows the normalized errors for all the cases, reiterating that all the models are a good fit to the measured fluorescence.

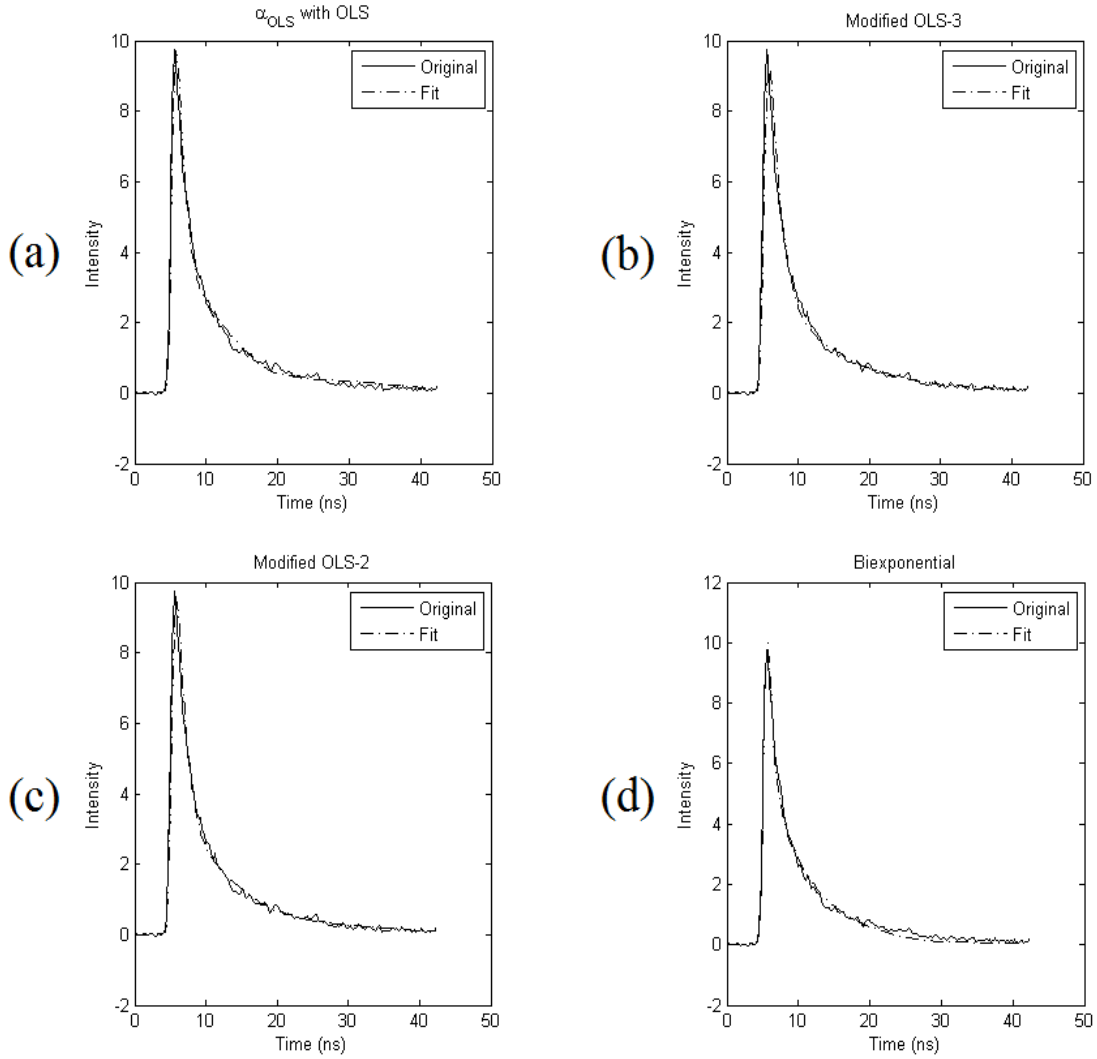

Figure 5: Measured Fluorescence and Convolved Fittings for the First Case. The "α_OLS with OLS" Method Fitting Depicts an Oscillatory Behavior. (a) "α_OLS with OLS", (b) "Modified OLS-3", (c) "Modified OLS-2", and (d) "Biexponential" Methods.

.

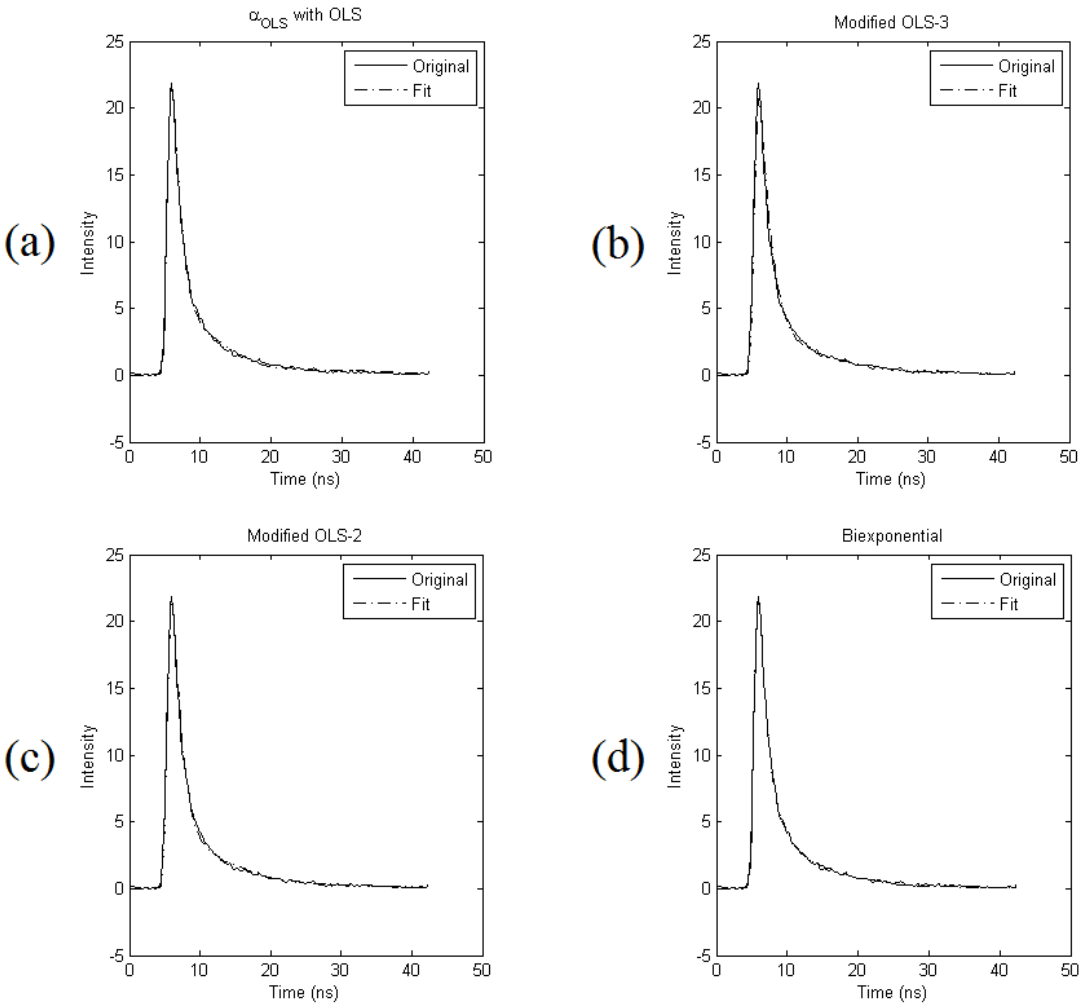

Figure 6: Measured Fluorescence and Convolved Fittings for the Second Case. The "α_OLS with OLS" Method Fitting Depicts an Oscillatory Behavior. (a) "α_OLS with OLS", (b) "Modified OLS-3", (c) "Modified OLS-2", and (d) "Biexponential" Methods.

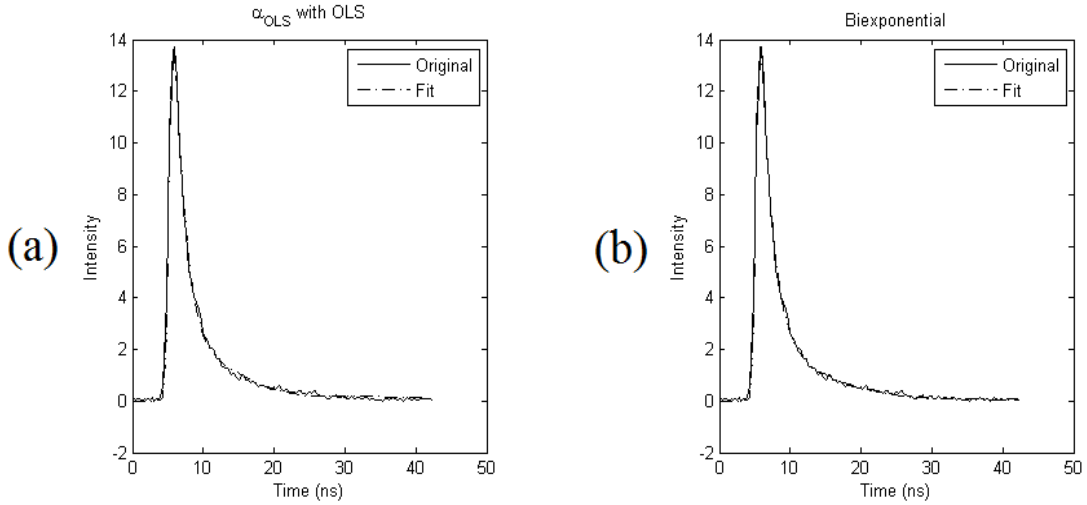

Figure 7: Measured Fluorescence and Convolved Fitting for the Third Case. (a) "α_OLS with OLS", "Modified OLS-3", and "Modified OLS-2" Methods and (b) the "Biexponential" Method.

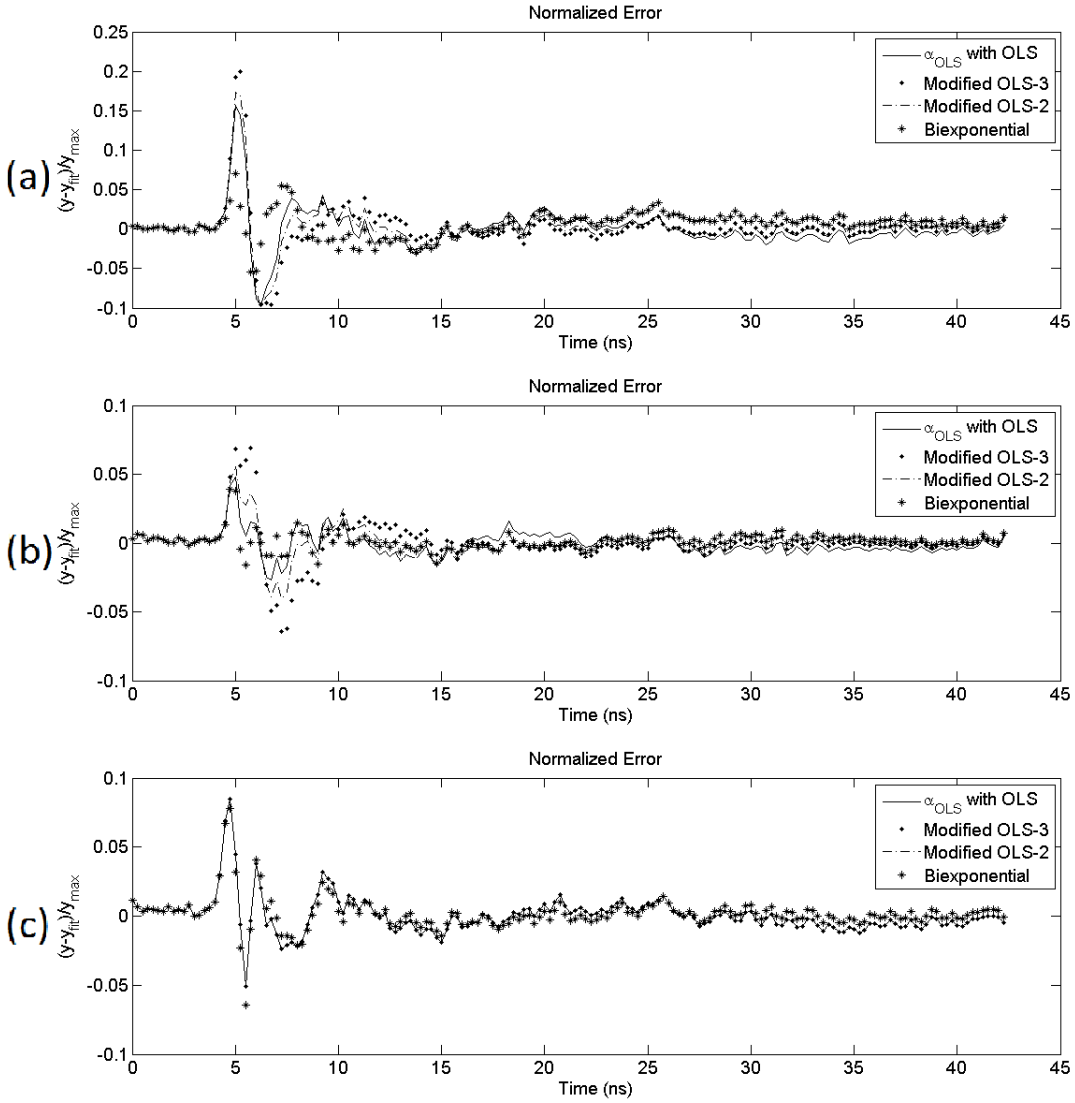

Figure 8: Normalized Error for (a) the First Case, (b) the Second Case, and (c) the Third Case.

The deconvolved exponential curves are shown in Figs. 9 – 11 for the three cases. . The first case (shown in Fig. 9) depicts a slight downward concavity for the "α_{OLS} with OLS" method deconvolution, shown in Fig. 9(a), between approximately 5ns and 12ns (see inset for magnified curve). Because a downward concavity represents a negative second derivative, the curve fails the third property listed for an exponential decay. The second case (shown in Fig. 10) depicts a sinusoidal behavior for the "α_{OLS} with OLS" method deconvolution, shown in Fig. 10(a), between approximately 12ns and 30ns. Because a sinusoid oscillates between higher and lower values, the curve fails the second and third properties listed for an exponential decay. The "Modified OLS-2" and "Modified OLS-3" method deconvolutions, however, do not fail the properties listed for an exponential decay, and the results are similar to the "Biexponential" method deconvolution. In the third case (shown in Fig. 11), the "α_{OLS} with OLS" method deconvolution follows all the listed properties of an exponential decay and is similar to the "Biexponential" method deconvolution.

This is 7 point font

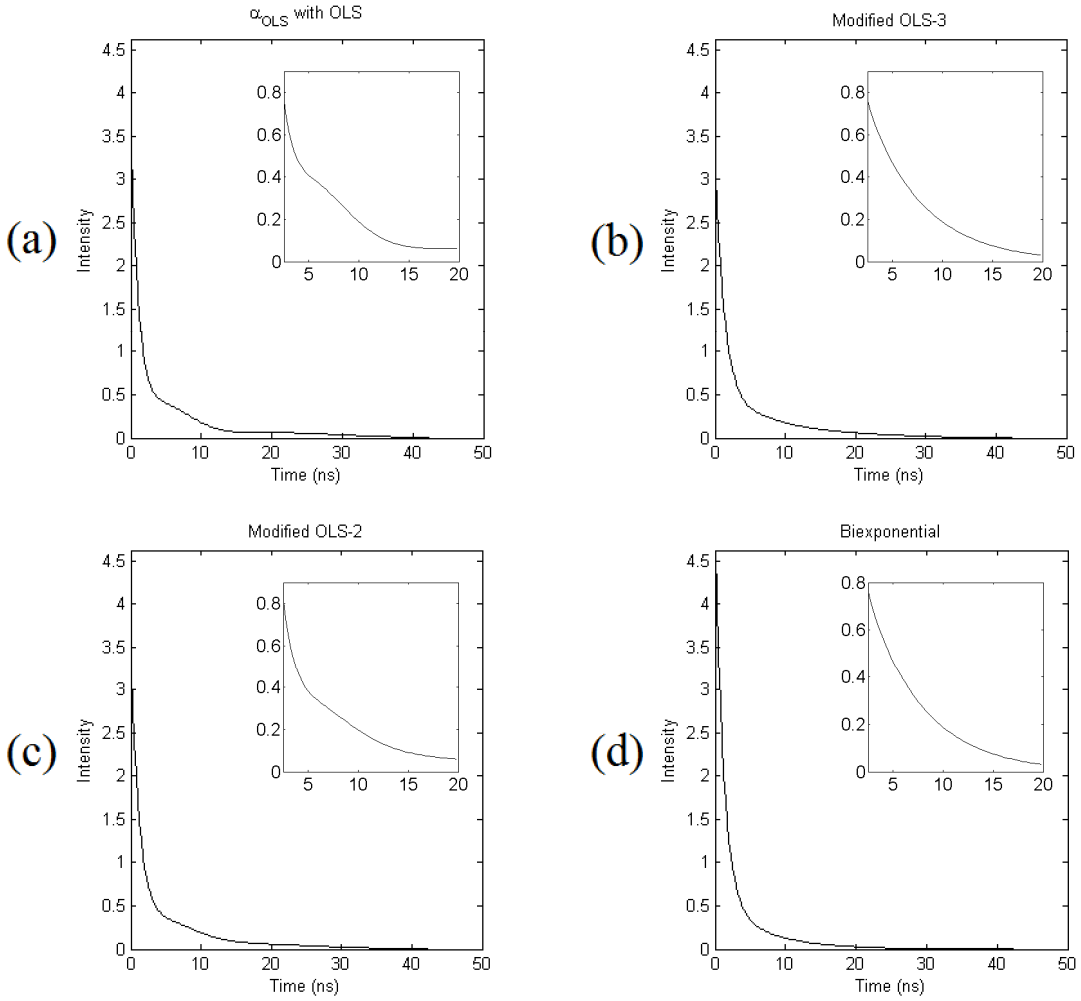

Figure 9: Deconvolved Fluorescence Decay Estimations for the First Case. The "α_OLS with OLS" Method Deconvolution Depicts a Negative Concavity. (a) "α_OLS with OLS", (b) "Modified OLS-3", (c) "Modified OLS-2", and (d) "Biexponential" Methods. Inset: Curve Between 2.5ns and 20ns.

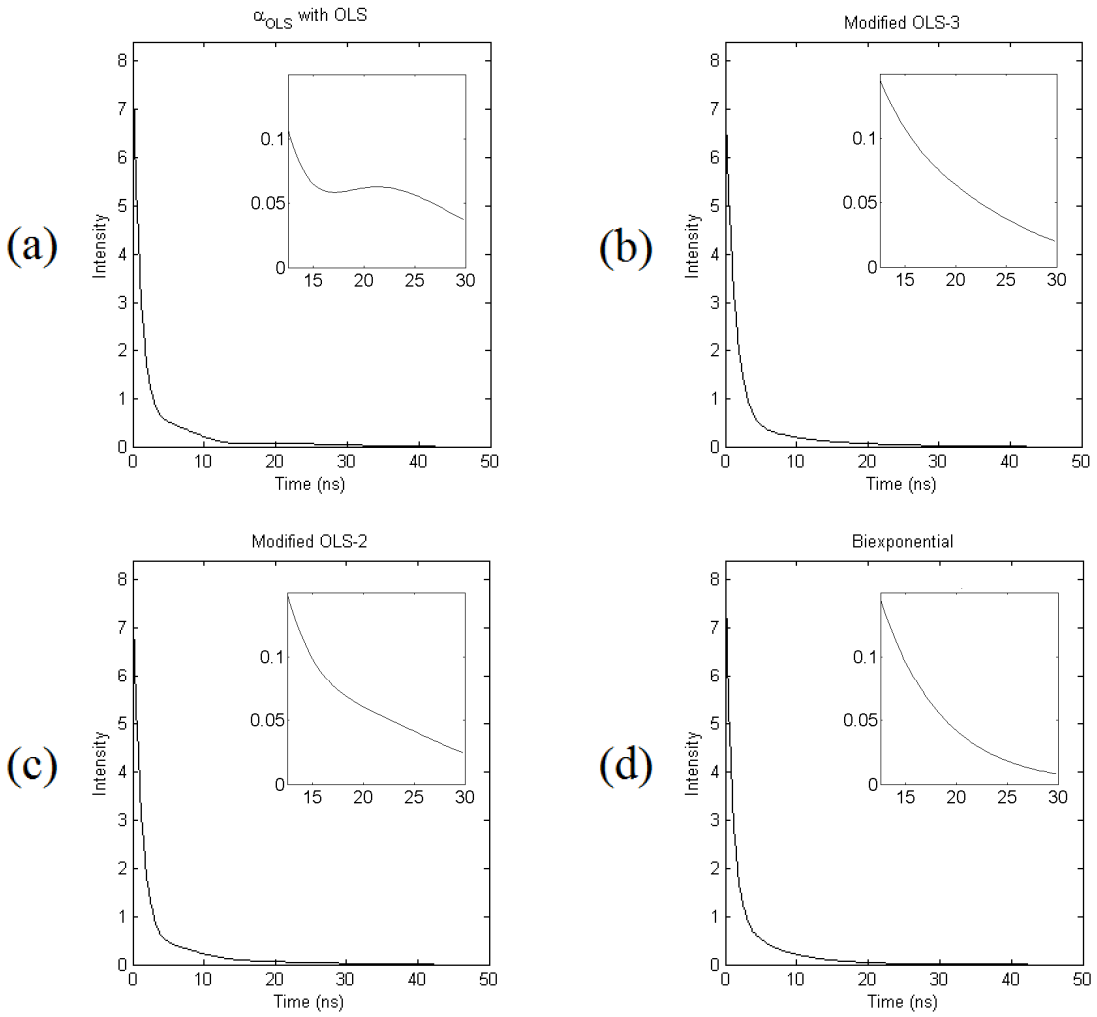

Figure 10: Deconvolved Fluorescence Decay Estimations for the Second Case. The "α_OLS with OLS" Method Deconvolution Depicts a Sinusoidal Behavior. (a) "α_OLS with OLS", (b) "Modified OLS-3", (c) "Modified OLS-2", and (d) "Biexponential" Methods. Inset: Curve Between 12.5ns and 30ns.

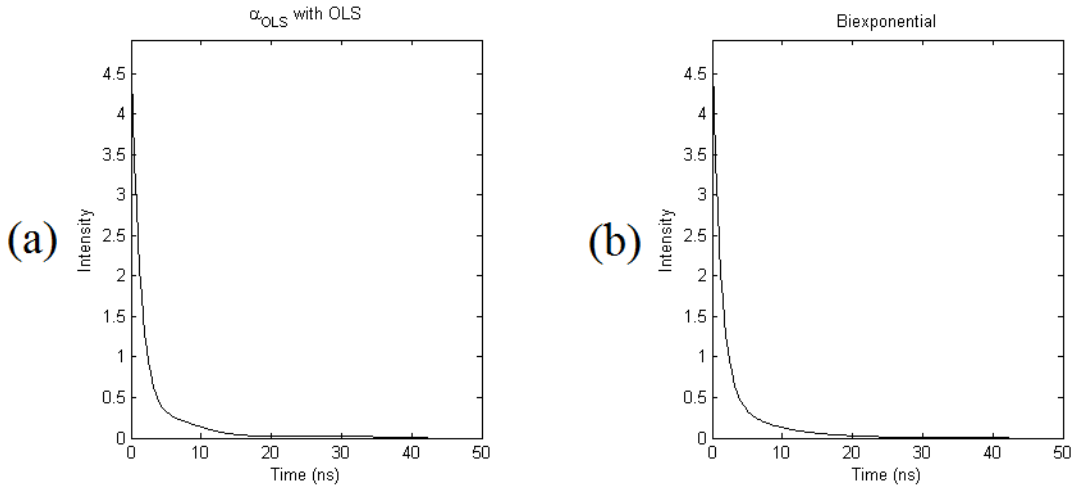

Figure 11: Deconvolved Fluorescence Decay Estimations for the Third Case. (a) "α_OLS with OLS", "Modified OLS-3", and "Modified OLS-2" Methods and (b) the "Biexponential" Method.

4. SUMMARY AND CONCLUSIONS

In this study, we have demonstrated that combining multiple deconvolution techniques results in faster and more accurate deconvolution of recorded fluorescence decays in FLIM. The use of the automated method for global Laguerre parameter optimization results in a fast deconvolution while the use of the constraint on the Laguerre Basis Functions (LBFs) insures proper deconvolution. The use of the LBFs also allows for simultaneous deconvolution of a large data set. The constraint on the LBFs prevents overfitting of the recorded fluorescence decays, thereby removing the effect of noise from the deconvolved curve. Therefore, neither the number of exponentials nor the Laguerre parameter value requires *a priori* assumptions. The efficacy of the difference in the average lifetime maps, though, has yet to be determined with respect to tissue classification.

With respect to the deconvolutions, the “Modified OLS-2” and “Modified OLS-3” method deconvolutions are similar to each other. The “Modified OLS-3” method deconvolutions, however, tend to look less piecewise and more smooth than the “Modified OLS-2” method deconvolutions. While either method is feasible, we have not been able to identify a requirement for using the third derivative when the second derivative is available.

Furthermore, the current work requires the fluorescence signal to decay down to zero with time. If the recorded signal does not decay down towards zero by the end of the acquisition time period, the algorithm will force the convolved fit to do so. This “forcing” will result in poorly modeled fluorescence signals with large normalized errors. An example of this situation is recorded a fluorescence signal with a relatively long average lifetime (ex. ~14ns) for a relatively shorter time period (ex. ~50ns). Correlating average lifetime values to required signal acquisition time period, however, is outside the scope of this paper.

REFERENCES

1. L. Marcu, J. A. Jo, Q. Fang, T. Papaioannou, T. Reil, J. H. Qiao, J. D. Baker, J. A. Freischlag, and M. C. Fishbein, “Detection of rupture-prone atherosclerotic plaques by time-resolved laser-induced fluorescence spectroscopy," Atherosclerosis **204**, 156-164 (2009).

2. M. C. Skala, K. M. Riching, A. Gendron-Fitzpatrick, J. Eickhoff, K. W. Eliceiri, J. G. White, and N. Ramanujam, "In vivo multiphoton microscopy of NADH and FAD redox states, fluorescence lifetimes, and cellular morphology in precancerous epithelia," Proc Natl Acad Sci U S A **104**, 19494-19499 (2007).

3. Q. Y. Fang, T. Papaioannou, J. A. Jo, R. Vaitha, K. Shastry, and L. Marcu, "Time-domain laser-induced fluorescence spectroscopy apparatus for clinical diagnostics," Rev Sci Instrum **75**, 151-162 (2004).

4. K. Arakawa, K. Isoda, T. Ito, K. Nakajima, T. Shibuya, and F. Ohsuzu, "Fluorescence analysis of biochemical constituents identifies atherosclerotic plaque with a thin fibrous cap," Arterioscler Thromb Vasc Biol **22**, 1002-1007 (2002).

5. N. Ramanujam, "Fluorescence spectroscopy of neoplastic and non-neoplastic tissues," Neoplasia **2**, 89-117 (2000).

6. S. Shrestha, B. E. Applegate, J. Park, X. Xiao, P. Pande, and J. A. Jo, "A novel high-speed multispectral fluorescence lifetime imaging implementation for in vivo applications," Opt Lett **35**, 2558-2560 (2010).

7. P. Pande, and J. A. Jo, "Automated analysis of fluorescence lifetime imaging microscopy (FLIM) data based on the laguerre deconvolution method," IEEE Trans Biomed Eng **58**, 172-181 (2011).

8. J. A. Jo, Q. Fang, and L. Marcu, "Ultrafast method for the analysis of fluorescence lifetime imaging microscopy data based on the Laguerre expansion technique," IEEE J Select Topics Quantum Electron **11**, 835-845 (2005).

9. V. Z. Marmarelis, "Identification of nonlinear biological-systems using laguerre expansions of kernels," Ann Biomed Eng **21**, 573-589 (1993).

10. L. J. D. William R. Ware, Thomas L. Nemzek, "Deconvolution of fluorescence and phosphorescence decay curves. Least-squares method," J Phys Chem **77**, 2038-2048 (1973).

11. K. C. Lee, J. Siegel, S. E. Webb, S. Leveque-Fort, M. J. Cole, R. Jones, K. Dowling, M. J. Lever, and P. M. French, "Application of the stretched exponential function to fluorescence lifetime imaging," Biophys J **81**, 1265-1274 (2001).

12. V. K. Ramanujan, J. A. Jo, G. Cantu, and B. A. Herman, "Spatially resolved fluorescence lifetime mapping of enzyme kinetics in living cells," J Microsc **230**, 329-338 (2008).

13. J.-M. I. Maarek, W. Snyder, and W. Grundfest, “Time-resolved laser-induced fluorescence of arterial wall constituents: Deconvolution algorithm and spectro-temporal characteristics,” Proc SPIE **2980**, 278 (1997).

14. Jo, J.A.; Fang, Q.; Papaioannou, T.; Marcu, L., "Novel ultra-fast deconvolution method for fluorescence lifetime imaging microscopy based on the Laguerre expansion technique," Engineering in Medicine and Biology Society, 2004. IEMBS '04. 26th Annual International Conference of the IEEE **1**, 1271-1274, 1-5 Sept. 2004. San Francisco, CA.

15. V.K. Ramanujan, J.A. Jo, G. Cantu, and B.A. Herman, “Spatially resolved fluorescence lifetime mapping of enzyme kinetics in living cells,” J Microsc **230**, 329–338 (2008).

16. D.S. Elson, J.A. Jo, and L. Marcu, “Miniaturized side-viewing imaging probe for fluorescence lifetime imaging (FLIM): validation with fluorescence dyes, tissue structural proteins and tissue specimens,” New J Phys **9** (2007).

17. J. Liu, Y. Sun, J. Qi, and L. Marcu, “A novel method for fast and robust estimation of fluorescence decay dynamics using constrained least-squares deconvolution with Laguerre expansion,” Phys Med Biol, **57**, 843-865 (2012).

18. J. Brandon, C. Conti, L. Goldstein, J. DiGiovanni, and I. Gimenez-Conti, "Carcinogenic effects of MGP-7 and B[a]P on the hamster cheek pouch.," Toxicol Pathol **37**, 733-740 (2009).

19. M. Abramowitz and I.A. Stegun, “Handbook of mathematical functions : with formulas, graphs and mathematical tables,” Dover Publications, New York: 1973.

20. C.L. Lawson and R.J. Hanson, “Solving least squares problems,” Prentice-Hall, Englewood Cliffs, NJ: 1974.